Available online at www.sciencedirect.com
ScienceDirect
Journal of Sound and Vibration 300 (2007) 292–315
JOURNAL OF SOUND AND VIBRATION
www.elsevier.com/locate/jsvi

Vibration control of simply supported beams under moving loads using fluid viscous dampers

P. Museros[a,*], M.D. Martinez-Rodrigo[b]

[a]*Departamento de Mecánica de Estructuras, Escuela Técnica Superior de Ingenieros de Caminos, Universidad de Granada, 18071 Granada, Spain*

[b]*Departamento de Ingeniería Mecánica y Construcción, Universidad Jaume I, 12071 Castellón, Spain*

Received 27 June 2005; received in revised form 31 July 2006; accepted 9 August 2006
Available online 27 October 2006

Abstract

In this article, a new alternative for reducing the resonant vibration of simply supported beams under moving loads is presented and numerically evaluated. The strategy proposed is based on the use of linear fluid viscous dampers that connect the beam carrying the loads (main beam) and an auxiliary beam placed underneath the main one. Our research study shows that the resonant response of the main beam can be drastically reduced with this type of device. Firstly, the main beam equipped with the damping system is subjected to a sinusoidal excitation and analysed with a view to discovering the dampers which minimise the overall dynamic response at resonance. In this way, a closed-form expression of the optimal damper constants is obtained for minimising the vertical acceleration, and a slightly different one for minimising the vertical displacement. These expressions are then applied to real bridges subjected to railway traffic, and their adequacy is proven for a wide range of circulating velocities. Finally, we compare the performance of the original structure with the performance of the one equipped with these optimal dampers. The results of our study prove their effectiveness and technical feasibility. The methodology proposed has potential applications for the reduction of the response of railway bridges subjected to the transit of high-speed trains.

1. Introduction

Regarding the analysis of simply supported beams subjected to moving loads, a crucial area of focus over the last 20 years has been the dynamic performance of railway bridges subjected to the transit of high-speed trains. The main reason for this growing interest is the widespread construction of new high-speed lines as well as the reuse of older lines for higher operating train velocities.

Fast trains can induce resonance situations in railway bridges, especially in those where the main structural elements are simply supported beams. Resonance takes place when the time interval between the passages of repeated groups of loads over a certain section of the bridge is a multiple of one of its natural periods. Furthermore, a second type of resonance phenomenon related to the dynamic stability of the beam can take

*Corresponding author. Tel.: +34 958240768; fax: +34 958249959.
E-mail address: pmuseros@ugr.es (P. Museros).

0022-460X/$ - see front matter © 2006 Elsevier Ltd. All rights reserved.
doi:10.1016/j.jsv.2006.08.007

place at very high speed. In practice, such speed is unattainable by modern trains (see Ref. [1]) and therefore, this kind of resonance will not be considered in this article.

As the train velocity approaches resonant velocity, a dynamic amplification of the structural response is to be expected, and in particular, inadmissible vertical accelerations may occur on the bridge. This can cause passenger discomfort, a reduction of the service life of the bridge, ballast deconsolidation, and subsequent risk of derailment. This kind of behaviour has been reported by members of the D-214 Committee of the European Rail Research Institute [2,3]. It is thus essential to control the resonant vibration of such structures under the circulation of trains.

The possibility of mitigating the resonant vibration of simple beams by increasing the overall structural damping with passive energy dissipation devices is evaluated in this paper. More specifically, the authors propose the use of linear fluid viscous dampers (FVDs). These dampers are to be installed by connecting the beam supporting the passage of the loads (*main beam* in what follows) to an *auxiliary beam,* which is most often placed underneath the main one.

Despite the fact that vibration control systems have been applied to reduce the dynamic response of structures since the 1960s, only a few authors have addressed the practical application of this technology to beams or bridges under the action of moving vehicles.

The application of tuned mass dampers (TMDs) to the train-induced vibration control of high-speed railway bridges is described in references [4–7]. Kwon et al. [4] investigate the effectiveness of a passive TMD installed at the mid-span section of a bridge with three spans of 40 m. The TMD parameters are obtained following Den Hartog's optimum tuning conditions [8]. The authors conclude that the maximum reduction of the vertical bridge displacement reaches 21%, whereas the vertical acceleration remains virtually unchanged. They attribute this to the fact that the vehicle passage time on the bridge is too short to build up the needed TMD vibrating regime.

Wang et al. [5] study the retrofit of two 30 and 40 m span simply supported bridges from the Taiwan High-Speed Railway system under the circulation of various train models. They tune the TMD parameters so that the frequency of the damper coincides with the modal frequency whose contribution needs to be mitigated, and locate the TMD at the maximum modal amplitude section. The authors conclude that the damping system has good control efficiency when the train travels at resonant speeds. They also discuss the detuning problems related to the exact natural frequency of the bridge and the variability of this frequency over time when vehicle–bridge interaction is accounted for. Regarding cable-stayed bridges, Yau and Yang [6] propose the installation of a particular hybrid TMD system to suppress the vibrations associated with several frequencies. The system consists of several subsystems, each of which is tuned to one dominant frequency. Finally, Das and Dey [7] study the effects of installing TMDs on bridges subjected to random excitations. These authors conclude that TMD arrangement has little effect on the response reduction when all the devices are tuned to the frequency of only one mode and that a TMD arrangement tuned to more than one mode is efficient as long as the structural frequencies are closely spaced.

Aside from passive TMDs, Minsili et al. [9] apply slotted friction connections to bridges for controlling running trains and earthquake excitations. They point out that this alternative reduces structural displacements to a great extent, but that the vertical accelerations may be even higher than the unretrofitted ones due to the nature of the forces introduced in the structure. Choo et al. [10] propose the retrofit of composite bridges with viscoelastic (VE) dampers. They carry out an experimental programme using acrylic rubber in order to dissipate energy through shear deformation, and adjust a numerical constitutive model for this material. The authors prove both numerically and experimentally that the device is able to raise the overall damping ratio, and this causes the structural response to fall below the permitted levels. The lengths of the bridges studied range from 40 to 60 m.

A few authors have addressed the use of pure viscous dampers to reduce the amplification in beams traversed by moving loads. Oliveto et al. [11] and Greco and Santini [12] solve the dynamic problem of a continuous beam with two end rotational viscous dampers under the circulation of a single load by using an extension of the complex mode superposition method. They conclude that the dampers' effectiveness is strongly dependant on the load speed and prove that in the relevant range of velocities, a considerable reduction of the dynamic response of the beam is to be expected if the dampers' constants are selected properly. Nevertheless, to the authors' knowledge, this type of damper has never been previously applied to the study of high-speed load traffic.

From a different perspective, but also relevant to the application of FVDs, some researchers have investigated the optimisation of linear dampers to be installed in structures and mechanical systems. Krenk [13] obtains the optimal devices for the beam treated in Refs. [11,12] from the complex modes of the system. In this paper Krenk presents a general procedure for solving the damped eigenvalue problem of continuous systems. Furthermore, this author shows that the orthogonality properties of the complex modes enable the transformation of the forced equations of motion to an uncoupled set of modal equations in a way similar to classical modal analysis. Also, Main and Krenk [14] use approximate complex modes to derive optimised viscous dampers for discrete systems. They interpolate the damped modes from two limiting cases (the undamped system and the system obtained by locking all dampers), and present a procedure for calculating the complex frequencies. The optimal sizing and placement of the dampers for each mode is determined on the basis of this formulation.

We have selected FVDs, as compared to other passive energy dissipation devices, because FVDs dissipate energy at a wide scope of frequency ranges, and not only at narrow ranges like TMDs. As a result, they do not present tuning and detuning drawbacks. A further advantage is the fact that dissipative devices based on friction or yielding increase replacement operations and maintenance costs. In contrast, some FVDs are equipped with labyrinth seals which eliminate mechanical friction, and allow them to undergo an enormous number of cycles before they have to be replaced. Moreover, since in FVDs the maximum force and maximum displacement are out of phase, additional forces introduced in the structure are small when compared to other procedures.

More specifically, the solution that we are proposing is a viable alternative for the retrofit of existing bridges that show inadequate dynamic performance under the passage of fast trains. For this reason, throughout the rest of the article the damping system will also be referred to as *retrofitting system*.

2. Configuration of the damping system

The dissipative system to be installed on the beam supporting the passage of the loads consists of two main elements. The first element is an auxiliary, simply supported beam which in typical applications is generally located underneath the main beam. The second element is a set of FVDs linking the vertical motion of certain sections of the main beam and the auxiliary one. Our attention here is focused on mitigating the flexural vibrations of the main beam when the train of moving loads induces a resonance situation. For this reason, we use a planar model for analysing the retrofit configuration proposed (see Fig. 1). The loads acting on the structure are assumed to be constant-valued, i.e. vehicle–bridge interaction effects are neglected.

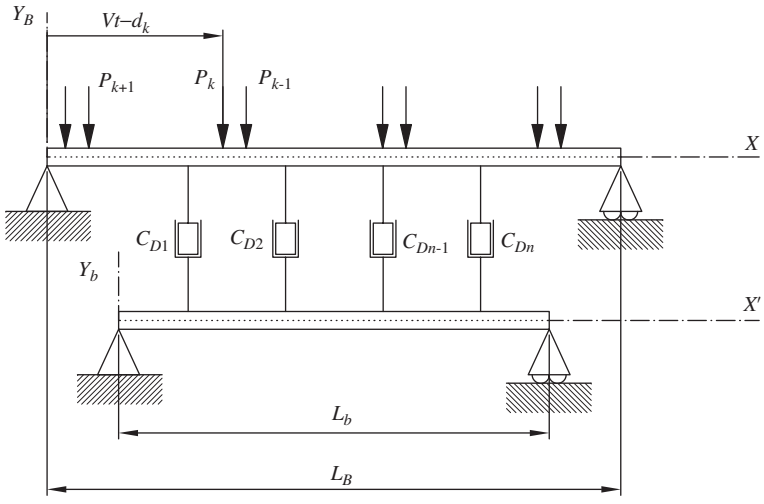

Fig. 1. Main beam and retrofitting system.

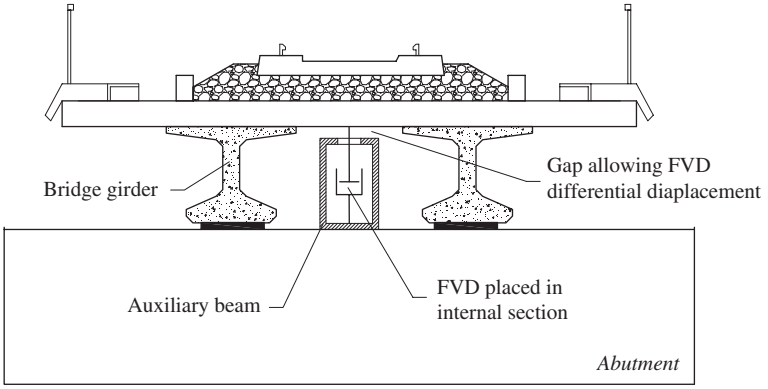

Fig. 2. Retrofit configuration for a concrete girder bridge.

The consequences of this hypothesis are examined in Sections 4.2 and 5.4. Also, the main and auxiliary beams are assumed to rest directly on the abutments without any intermediate elastic bearing.

The torsional oscillations experienced by beams subjected to eccentric moving loads are not analysed in this study. Consequently, the results presented here are not applicable to either multitrack railway bridges or single-track skewed railway bridges. The analysis of multitrack bridges retrofitted with FVDs generally requires the use of three-dimensional models, and will be the subject of future research work. However, it should be emphasised that single-track non-skewed bridges, and in particular, medium to short-span ones are some of the most unfavourable cases found in practice. As a consequence of their low total mass, this type of structure may undergo severe resonant oscillations under the passage of fast trains, thus generating highly demanding situations for any dissipative system.

Fig. 2 shows a possible configuration of the auxiliary beam and dampers installed in a single-track railway bridge. The dampers link the lower side of the slab and the interior of the lower flange of an auxiliary beam with a hollow rectangular cross-section. The auxiliary beam is simply supported on the abutments at the outermost sections of the bridge. If the clearance below the bridge is to be maintained, the upper flange of the auxiliary beam will require drilling and, occasionally, local strengthening. As will be shown in Section 5, the concentrated loads transmitted by the dampers are rather low in comparison to the allowable punching loads for typical reinforced concrete slabs. Other suitable configurations could be adopted in each particular case.

3. Governing parameters and influence on the response

3.1. Equations of motion of a simple beam under moving loads

The partial differential equation governing the flexural behaviour of a simply supported beam subjected to a train of concentrated loads can be found in the work of various authors such as Frýba [1,15], Olsson [16], Yang et al. [17], and Museros and Alarcón [18]. Neglecting the effects of shear deformation and rotary inertia, and considering that the loads are aligned with the axis of symmetry of the cross-section (Y-axis), the governing equation can be written as

$$m\frac{\partial^2 y}{\partial t^2}+\frac{\partial^2}{\partial x^2}\left(EI\frac{\partial^2 y}{\partial x^2}\right)=q(x,t). \tag{1}$$

In Eq. (1), the following notation is used: m is the mass per unit length; $y=y(x, t)$ is the transverse displacement of any beam section at time t; x refers to the longitudinal coordinate; E is the modulus of elasticity; I is the second moment of area of the cross-section; and $q(x, t)$ stands for the distributed load per unit length acting at time t (positive if directed upwards).

The deformed shape is expressed as a linear combination of a family of sines $\phi_j(x)$ as in Eq. (2):

$$y(x,t)=\sum_{j=1}^{N_{\mathrm{mod}}}\xi_j(t)\phi_j(x)=\sum_{j=1}^{N_{\mathrm{mod}}}\xi_j(t)\sin\left(\frac{j\pi x}{L}\right), \tag{2}$$

where N_{mod} stands for the number of modes considered, $\xi_j(t)$ is the amplitude of the jth mode, and L is the length of the beam. The loads are represented by means of Dirac delta functions acting at $x=Vt-d_k$, where V is the constant train speed, and d_k is the original distance from the kth load to the beginning of the beam. Thus, $q(x, t)$ may be expressed as follows:

$$q(x,t)=-\sum_{k=1}^{N_P}\left(H\left(t-\frac{d_k}{V}\right)-H\left(t-\frac{d_k+L}{V}\right)\right)P_k\delta(x-(Vt-d_k)), \tag{3}$$

where N_P is the total number of axle loads; P_k is the value of the kth load; and $H(t-t_0)$ is the Heaviside unit function acting at time t_0. When Eqs. (2) and (3) are introduced in Eq. (1), and multiplication by the nth sine function $\phi_n(x)$ and integration along span L are carried out, the nth modal equation of motion is obtained. To this end, the mass per unit length m and the flexural stiffness EI are assumed to be constant along the beam. Introducing a modal viscous damping ratio ζ_n, the modal equation of motion is expressed as

$$\ddot{\xi}_n(t)+2\zeta_n\omega_n\dot{\xi}_n(t)+\omega_n^2\xi_n(t)=\frac{-2}{mL}\sum_{k=1}^{N_P}\left(H\left(t-\frac{d_k}{V}\right)-H\left(t-\frac{d_k+L}{V}\right)\right)\times P_k\sin\frac{n\pi(Vt-d_k)}{L}, \tag{4}$$

where over-dots indicate differentiation with respect to time, and ω_n represents the beam nth circular frequency in rad/s:

$$\omega_n=\left(\frac{n\pi}{L}\right)^2\sqrt{\frac{EI}{m}}. \tag{5}$$

3.2. Governing equations of the beam equipped with fluid viscous dampers and subjected to moving loads

When the auxiliary beam is introduced and both beams are connected by means of FVDs, the equations of motion must be modified accordingly. The auxiliary beam is modelled on the assumption of Bernoulli–Euler behaviour, and only flexural modes are accounted for. Therefore, the governing equation for the nth mode of the auxiliary beam is analogous to Eq. (4), but introducing dampers forces acting at fixed positions. These forces must also be introduced with opposite signs in the equations of the main beam. The resulting equations of motion for the nth mode of the main and auxiliary beams are as follows:

$$\ddot{\xi}_n^B(t)+2\zeta_n^B\omega_n^B\dot{\xi}_n^B(t)+\left(\omega_n^B\right)^2\xi_n^B(t)=\frac{-2}{m_BL_B}\sum_{i=1}^{N_D}\left[\sin\frac{n\pi\,x_{Di}}{L_B}\,C_{Di}\,\dot{y}_{\mathrm{rel},i}(t)\right]+f_n(t),$$

$$\ddot{\xi}_n^b(t)+2\zeta_n^b\omega_n^b\dot{\xi}_n^b(t)+\left(\omega_n^b\right)^2\xi_n^b(t)=\frac{2}{m_bL_b}\sum_{i=1}^{N_D}\left[\sin\frac{n\pi\,x'_{Di}}{L_b}\,C_{Di}\,\dot{y}_{\mathrm{rel},i}(t)\right],$$

$$\dot{y}_{\mathrm{rel},i}(t)=\sum_{j=1}^{N_{\mathrm{mod}}^B}\sin\frac{j\pi\,x_{Di}}{L_B}\,\dot{\xi}_j^B-\sum_{j=1}^{N_{\mathrm{mod}}^b}\sin\frac{j\pi\,x'_{Di}}{L_b}\,\dot{\xi}_j^b,$$

$$f_n(t)=-\frac{2}{m_BL_B}\sum_{k=1}^{N_P}\left(H\left(t-\frac{d_k}{V}\right)-H\left(t-\frac{d_k+L_B}{V}\right)\right)P_k\sin\frac{n\pi(Vt-d_k)}{L_B}. \tag{6}$$

The notation in Eq. (6) is analogous to Eqs. (2) and (4), but with superscripts and subscripts B and b, which indicate magnitudes associated to the main and auxiliary beam, respectively. Moreover, N_D is the total number of FVDs, and C_{Di} is the constant of the ith damper. The location of the ith damper is designated as x_{Di} along the X-axis of the main beam, and as x'_{Di} along the X'-axis of the auxiliary beam. Finally, $y_{\mathrm{rel},i}(t)$ is the relative vertical displacement or elongation of the ith FVD. From Eq. (6) it can be seen that if the modal

system of equations is written in matrix form, the load term associated with the forces exerted by the FVDs generally gives rise to a full damping matrix.

3.3. Non-dimensional formulation of the beam equipped with fluid viscous dampers and subjected to a sinusoidal excitation

This article focuses on the reduction of the resonant response of the main beam, and therefore, the system shown in Fig. 1 will be first analysed under the action of a harmonically varying force. This kind of excitation captures the essential features of the system response at resonance.

In practical applications, resonance induced by constant moving loads is a problem typical of bridges subjected to the passage of fast trains. Museros and Alarcón [18] show that even if resonance of the second bending mode can take place in certain cases, in single-track bridges it is most likely that resonance will be related to oscillations of the first bending mode. This is a consequence of the maximum speed attainable by modern high-speed trains. Under such circumstances, the influence of modes other than the one undergoing resonance can be disregarded in the computation of the main beam response.

The oscillations of the first mode of the main beam at resonance tend to create a symmetric distribution of damper forces with respect to the mid-span section. These forces excite the movement of the auxiliary beam which, consequently, can be initially analysed only taking into account the contribution of its first bending mode. The viability of disregarding the second and higher modes of the beams in the calculation of the optimal parameters of the damping system is subsequently verified with two real examples (see Section 5).

In what follows, it will be assumed that the lengths of both beams are equal, $L_B = L_b = L$ and that the main beam and auxiliary beam are vertically aligned so that $x_{Di} = x'_{Di}$, $i = 1, 2, \ldots, N_D$. These hypotheses are the most relevant ones for real applications because it is most likely that in actual bridges, the auxiliary beam or beams are supported at the original abutments or close to them. If only the first mode of both beams is taken into account, any number of FVDs located at different sections is equivalent to a single equivalent FVD located at mid-span. Fig. 3a shows the configuration of the system and the associated notation. The expression of the constant of the equivalent damper C_D is

$$C_D = \sum_{i=1}^{N_D} C_{Di} \sin^2\left(\frac{\pi x_{Di}}{L}\right). \tag{7}$$

The system shown in Fig. 3a is subjected to a point force, which varies harmonically in order to analyse its behaviour under resonance conditions. The assembly constitutes the two-degree-of-freedom system shown in Fig. 3b, where ξ_B and ξ_b, correspond to the first modal amplitudes of the main beam and auxiliary beam,

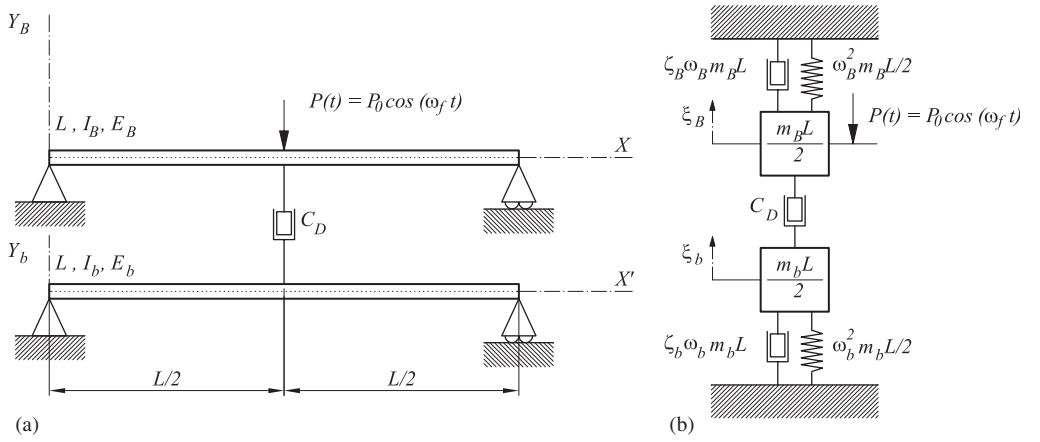

Fig. 3. (a) Diagram of the retrofitted beam subjected to a sinusoidal load applied at mid-span. (b) Representation of the first flexural modes of vibration of the beams in modal space coordinates.

respectively. The equations of motion of the system are

$$\begin{bmatrix} 1 & 0 \\ 0 & 1 \end{bmatrix} \begin{pmatrix} \ddot{\xi}_B \\ \ddot{\xi}_b \end{pmatrix} + \begin{bmatrix} 2\zeta_B\omega_B + \dfrac{2C_D}{m_BL} & \dfrac{-2C_D}{m_BL} \\ \dfrac{-2C_D}{m_bL} & 2\zeta_b\omega_b + \dfrac{2C_D}{m_bL} \end{bmatrix} \begin{pmatrix} \dot{\xi}_B \\ \dot{\xi}_b \end{pmatrix} + \begin{bmatrix} \omega_B^2 & 0 \\ 0 & \omega_b^2 \end{bmatrix} \begin{pmatrix} \xi_B \\ \xi_b \end{pmatrix} = \begin{pmatrix} \dfrac{-2P_0}{m_BL}\cos(\omega_f t) \\ 0 \end{pmatrix}. \tag{8}$$

In Eq. (8), ω_B, ω_b represent the circular frequencies of the first bending mode of the beams; ζ_B, ζ_b are the corresponding damping ratios; and m_BL, m_bL, the total masses. P_0, ω_f are the amplitude and forcing frequency of the excitation, respectively. In order to solve Eq. (8) the following dimensionless ratios are defined:

$$\text{Frequency ratio}: \quad \eta = \omega_b/\omega_B, \tag{9a}$$

$$\text{Excitation frequency ratio}: \quad \Omega = \omega_f/\omega_B, \tag{9b}$$

$$\text{Mass ratio}: \quad \mu = m_b/m_B, \tag{9c}$$

$$\text{Supplemental damping ratio}: \quad \zeta_D = C_D/(m_BL\omega_B). \tag{9d}$$

Rewriting Eq. (8) in terms of the dimensionless ratios defined in Eqs. (9) yields

$$\begin{bmatrix} 1 & 0 \\ 0 & \mu \end{bmatrix} \begin{pmatrix} \ddot{\xi}_B \\ \ddot{\xi}_b \end{pmatrix} + 2\omega_B \begin{bmatrix} \zeta_B + \zeta_D & -\zeta_D \\ -\zeta_D & \zeta_b\eta\mu + \zeta_D \end{bmatrix} \begin{pmatrix} \dot{\xi}_B \\ \dot{\xi}_b \end{pmatrix} + \omega_B^2 \begin{bmatrix} 1 & 0 \\ 0 & \eta^2\mu \end{bmatrix} \begin{pmatrix} \xi_B \\ \xi_b \end{pmatrix} = \begin{pmatrix} \dfrac{-2P_0}{m_BL}\cos(\omega_f t) \\ 0 \end{pmatrix}. \tag{10}$$

If resonance is induced by a train of a large number of loads (as is the case of high-speed trains), the maximum response will correspond to the steady-state vibration. Therefore, the homogeneous or transient solution of Eq. (10) is neglected, and the forced or steady-state solution is obtained in complex form as follows:

$$\begin{pmatrix} \bar{\xi}_B \\ \bar{\xi}_b \end{pmatrix} = \left(-\omega_f^2\mathbf{M} + \mathrm{i}\omega_f\mathbf{C} + \mathbf{K}\right)^{-1} \begin{pmatrix} \dfrac{-2P_0}{m_BL} \\ 0 \end{pmatrix}, \tag{11}$$

where $\bar{\xi}_B$ and $\bar{\xi}_b$ are the complex amplitudes, $\mathbf{M}$, $\mathbf{C}$ and $\mathbf{K}$ are the mass, damping and stiffness modal matrices from Eq. (10), and $\mathrm{i} = \sqrt{-1}$. The moduli of $\bar{\xi}_B$ and $\bar{\xi}_b$ give the amplitudes of the response. In order to obtain a dimensionless representation, two modal amplifications are defined as the modulus of $\bar{\xi}_B$ and $\bar{\xi}_b$ divided by the static deflection caused by the concentrated load P_0 on the main beam

$$A_B = \frac{|\bar{\xi}_B|}{2P_0/(\omega_B^2 m_BL)}, \tag{12a}$$

$$A_b = \frac{|\bar{\xi}_b|}{2P_0/\omega_B^2 m_BL}. \tag{12b}$$

After some algebraic manipulation, the modal amplifications obtained are

$$A_B = \sqrt{\frac{4\Omega^2(\zeta_b\eta\mu + \zeta_D)^2 + \mu^2\left(\eta^2 - \Omega^2\right)^2}{E^2 + 4\Omega^2F^2}}, \tag{13a}$$

$$A_b = \frac{2\Omega\zeta_D}{\sqrt{E^2 + 4\Omega^2F^2}} \tag{13b}$$

being

$$E = \mu\left(1 - \Omega^2\right)\left(\eta^2 - \Omega^2\right) + 4\Omega^2\left(\zeta_D^2 - (\zeta_B + \zeta_D)(\zeta_b\eta\mu + \zeta_D)\right), \tag{13c}$$

$$F = \left(1 - \Omega^2\right)(\zeta_b\eta\mu + \zeta_D) + \mu(\zeta_B + \zeta_D)\left(\eta^2 - \Omega^2\right). \tag{13d}$$

The main beam modal acceleration is also of great interest because of its relation to ballast stability, mentioned in Section 1. In the steady state the amplitude of the acceleration a_B is

$$a_B = \left|\bar{\xi}_B\right|\omega_f^2 = \frac{2P_0}{m_BL}\Omega^2A_B. \tag{14}$$

Eq. (13) shows that the amplification of the main beam response A_B depends on the following six parameters: Ω, η, μ, ζ_D, ζ_b, ζ_B. Additionally, Eq. (14) shows that the modal acceleration of the main beam is inversely proportional to its total mass m_BL. The behaviour of the system in terms of these parameters is analysed in detail in the following section.

3.4. Parametric plots

The key variables of the problem that should be minimised are the main beam dynamic amplification and modal acceleration, A_B and a_B. In order to visualise how the governing parameters affect the main beam dynamic amplification, a number of plots are included in Fig. 4. The plots illustrate the response of the main

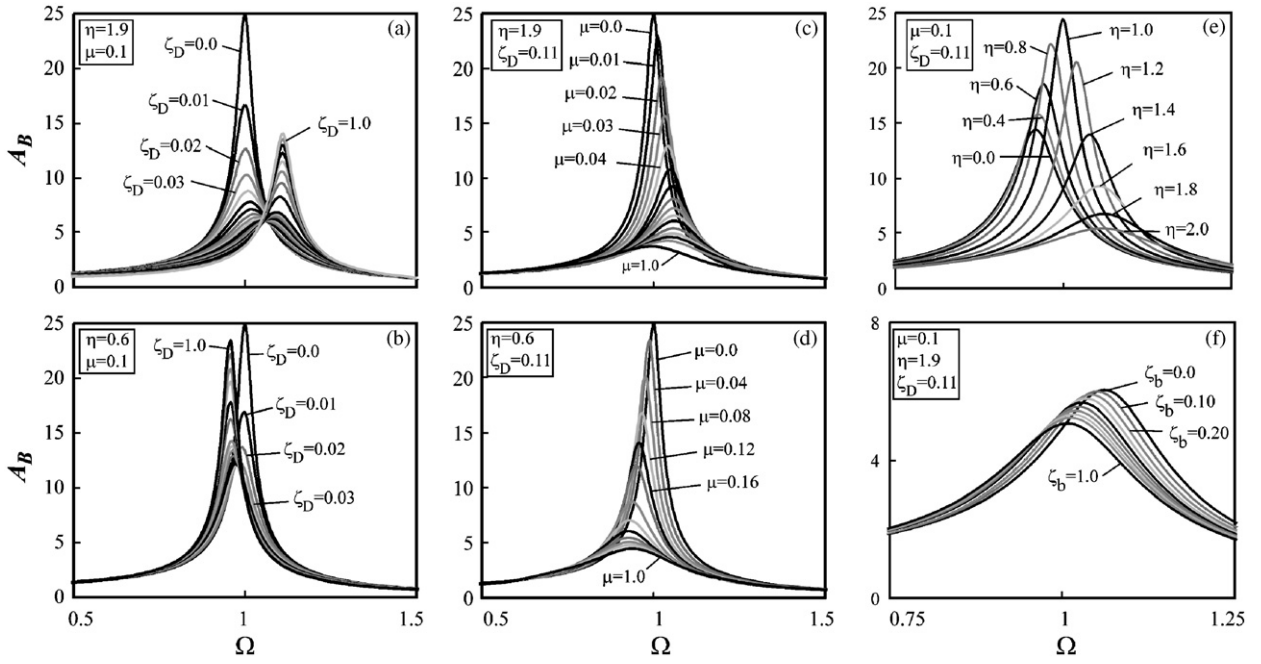

Fig. 4. Main beam amplification A_B versus Ω for different values of the governing parameters: (a) $A_B(\zeta_D)$ $\eta > 1$, (b) $A_B(\zeta_D)$ $\eta < 1$, (c) $A_B(\mu)$ $\eta > 1$, (d) $A_B(\mu)$ $\eta < 1$, (e) $A_B(\eta)$ and (f) $A_B(\zeta_b)$.

beam as a function of Ω for different values of one parameter, while maintaining the remaining parameters unmodified. In all the plots in Fig. 4, with the exception of Fig. 4f, the structural damping ratios of the main beam and the auxiliary beam are 2% and 0.5%, respectively.

Figs. 4a and 4b show the dynamic amplification of the main beam for different values of the supplemental damping ratio ζ_D. In both graphs, the mass ratio is equal to 0.1. When the damper constant equals zero, there is no interaction between the beams, and the main beam modal amplitude corresponds to the well-known response of a single degree of freedom (sdof) system. As the damper constant C_D increases along with ζ_D, the maximum response decreases, and the value of Ω for which resonance occurs (Ω_R in what follows) shifts sideways, depending on the value of the frequency ratio. If η is greater than one, as in Fig. 4a Ω_R increases, and if η is less than one, as in Fig. 4b Ω_R decreases. The maximum resonant amplification reduces monotonically with ζ_D until a minimum value is reached, and increases again if the damper constant keeps increasing. Consequently, for certain values of η and μ there is a value of ζ_D that leads to the minimum value of the maximum or resonant response. This minimum maximum occurs at a forcing frequency ratio which depends on μ and η as well. As the value of ζ_D tends to infinity, the two dof systems shown in Fig. 3b transform into a sdof system in which the two masses move jointly.

Figs. 4c and 4d gather plots of amplification A_B versus Ω for a constant value of ζ_D and η and different values of the mass ratio μ ($\zeta_D = 0.11$; $\eta = 1.9$ in Fig. 4c and $\eta = 0.6$ in Fig. 4d). The maximum amplification corresponds to a zero value of μ (i.e. the auxiliary beam is eliminated and the main beam vibrates according to its fundamental mode). As μ increases, the main beam amplification decreases monotonically. The minimum amplification occurs as μ tends to infinity. In that case, the main beam behaves as if its modal mass were attached through the external damper to a fixed reference, and the dynamic amplification tends to

$$A_B = \frac{1}{\sqrt{\left(1-\Omega^2\right)^2 + 4\Omega^2(\zeta_B+\zeta_D)^2}}. \tag{15}$$

Moreover, if a certain value of the mass ratio is exceeded, the response becomes almost insensitive to additional increments of this variable. In Fig. 4c, for instance, no significant change in A_B is observed if μ is given values greater than unity. A similar conclusion is applicable to Fig. 4d. Besides, as the mass ratio increases, Ω_R shifts to upper values (for $\eta > 1$ as in Fig. 4c) or to lower values (for $\eta < 1$ as in Fig. 4d); however, as μ tends to infinity, the frequency of the auxiliary beam does not influence the amplification of the main beam, and Ω_R is given by

$$\Omega_R = \sqrt{1-2(\zeta_B+\zeta_D)^2}. \tag{16}$$

In Fig. 4e, the amplification A_B is plotted versus Ω for fixed values of μ and ζ_D ($\mu = 0.1$, $\zeta_D = 0.11$), and several values of η. The maximum response occurs when the fundamental frequencies of both beams are the same ($\eta = 1$). In this case, both masses tend to vibrate in phase and the damper dissipates very little energy; indeed, if $\Omega = 1$ and structural damping is neglected the response tends to infinity. If the frequency ratio is reduced from $\eta = 1$ towards $\eta = 0$, the response of the main beam decreases and the peak values shift to the left as in Fig. 4e. However, the maximum reduction which occurs for $\eta = 0$ is much lower than the reduction obtained when $\eta > 1$. In the limit case $\eta = 0$ the mass of the auxiliary beam has neither associated stiffness nor structural damping. When the frequency ratio increases from $\eta = 1$, the main beam response decreases, and the peak values shift to the right. As η tends to infinity, the main beam ends up being attached through the external damper to a fixed reference; the dynamic amplification tends to Eq. (15), and Ω_R returns to Eq. (16). Finally, Fig. 4f shows that the main beam response diminishes when the auxiliary beam structural damping ζ_b increases. This result is consistent with different values of μ and η.

As regards the acceleration a_B, its evolution as a function of the governing parameters Ω, η, μ, ζ_D, ζ_b, ζ_B is essentially identical to that of the amplification A_B. Only two differences should be pointed out. First, the limit values of the acceleration are different from those of the dynamic amplification. More specifically, when Ω tends to zero, so does a_B, and for Ω tending to infinity, a_B tends to $2P_0/(m_B L)$. Secondly, the maximum amplification and acceleration take place at different values of Ω_R, a fact which is known to happen in sdof systems. However, for moderate damping ratios, the difference between the resonant frequencies corresponding to these two maximum values is small.

Because the system in Fig. 3b has two degrees of freedom, two resonant peaks could be expected in the response of both beams. However, the parametric study presented in this article focuses on the resonant response of the main beam produced by the coincidence between this element's natural frequency and the frequency of the excitation. From this perspective, it can be affirmed that in the range of interest of the non-dimensional parameters ($1.25 \leqslant \eta \leqslant 2.5$, $0.05 \leqslant \mu \leqslant 0.25$, $0 \leqslant \zeta_B \leqslant 0.05$, $0 \leqslant \zeta_b \leqslant 0.05$, $0 \leqslant \zeta_D \leqslant 0.20$) no second peak is perceptible in the response of the main beam.

Regarding the auxiliary beam, within the previously mentioned range of parameters, the resonant peak associated with its natural frequency only appears for very low values of ζ_D. Nevertheless, for the levels of supplemental damping required in order to reduce the main beam amplification to admissible values, this second resonant peak vanishes in the auxiliary beam as well. Resonance in the auxiliary beam is not a problem as such as long as the maximum stresses and displacements do not exceed admissible values. The numerical examples of very unfavourable scenarios (see Section 5) show that the stiffness requirements of the auxiliary beam avert any problems regarding the strength of this element.

The main conclusions that can be derived from the parametric analysis are (i) once the geometry and mass of the auxiliary beam are selected so that η and μ are defined, there is an optimum value of the damper constant which leads to the minimum maximum of the response of the main beam; (ii) for the effectiveness of the retrofitting system, η should be greater than one (values of η lower than 1.25 are generally of no interest in practical applications); (iii) there are no optimal values of η and μ. In other words, the dissipation capacity of the system increases with increasing values of any of these two parameters. The design strategy should be to select the smallest auxiliary beam, which along with its associated optimal damper, will provide enough energy dissipation to achieve the desired target performance.

4. Retrofitting system optimisation

In this section, the supplemental damping ratio ζ_D is optimised. The work of the European Rail Research Institute [19] shows that damping ratios in modern railway bridges are generally small (on the order of 1% or 2%), or even smaller in composite or metallic bridges. Therefore, in most practical cases an approximate solution to the problem can be obtained by assuming that structural damping is negligible in comparison to the dissipation introduced by the external FVD. This hypothesis allows the computation of a closed form expression for the optimal value of ζ_D. The subsequent numerical examples prove the soundness of this approach.

4.1. Optimal value of the supplemental damping ratio

Neglecting structural damping ($\zeta_B = \zeta_b = 0$), Eqs. (13a), (13c) and (13d) transform into

$$A_B = \sqrt{\frac{4\Omega^2\zeta_D^2 + \mu^2\left(\eta^2 - \Omega^2\right)^2}{\left(1-\Omega^2\right)^2\mu^2\left(\eta^2-\Omega^2\right)^2 + 4\Omega^2\zeta_D^2\left[1-\Omega^2+\mu\left(\eta^2-\Omega^2\right)\right]^2}}. \tag{17}$$

A comparison of Figs. 4a and 5 show the effect of structural damping on the response. Although the maximum amplification for low and high values of ζ_D at resonance reaches a much higher level when structural damping is not taken into account as in Fig. 5, two important facts must be highlighted. First, the difference between the maximum amplifications is much lower when ζ_D takes the optimal value. Particularly, in Fig. 4a the maximum amplification for the optimal ζ_D value is $A_B = 6.04$, whereas in Fig. 5, $A_B = 8.16$. This reveals that if structural damping is low and the optimal value of ζ_D is selected, the greater part of the energy at resonance is dissipated through the FVD. Secondly, if structural damping is neglected as in Fig. 5, A_B is independent of ζ_D at the value of Ω that corresponds to the minimum maximum. In order for this to happen, in Eq. (17) the following must be fulfilled:

$$\frac{4\Omega^2}{4\Omega^2\left[1-\Omega^2+\mu\left(\eta^2-\Omega^2\right)\right]^2} = \frac{\mu^2\left(\eta^2-\Omega^2\right)^2}{\left(1-\Omega^2\right)^2\mu^2\left(\eta^2-\Omega^2\right)^2}. \tag{18}$$

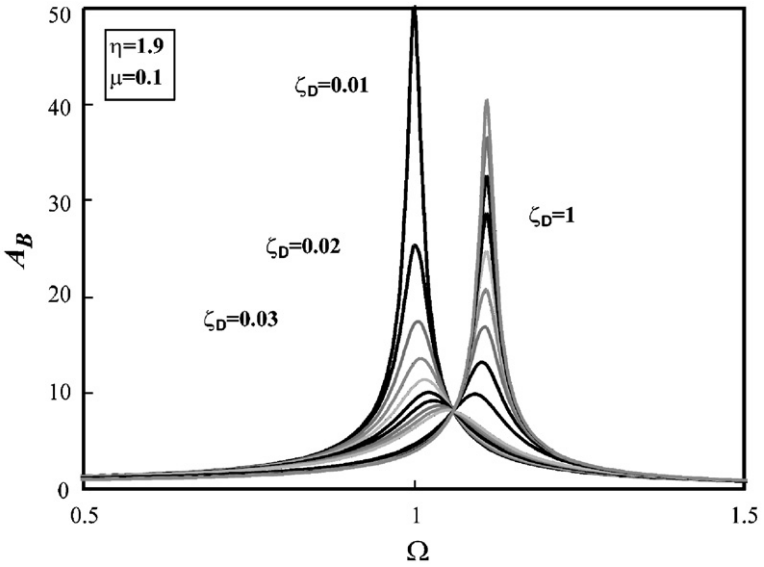

Fig. 5. Main beam amplification in terms of Ω for several values of ζ_D. Structural damping neglected.

The four solutions to Eq. (18) are

$$\Omega_R^{1*} = \frac{1}{2+\mu}\sqrt{(2+\mu)(2+\mu\eta^2)}, \tag{19a}$$

$$\Omega_R^{2*} = \frac{-1}{2+\mu}\sqrt{(2+\mu)(2+\mu\eta^2)}, \tag{19b}$$

$$\Omega_R^{3*} = \eta, \tag{19c}$$

$$\Omega_R^{4*} = -\eta. \tag{19d}$$

The solutions given by Eqs. (19b) and (19d) have no other meaning apart from the positive ones (19a) and (19c). Rather they are a consequence of the equal amplitude of the steady-state response that corresponds to positive and negative forcing frequencies with the same absolute value.

The solution Ω_R^{3*} given by Eq. (19c) has no importance for practical purposes because it does not correspond to the point where all curves in Fig. 5 coincide. Ω_R^{3*} corresponds to a point on the curve $A_B = A_B(\Omega)$ where A_B is independent of ζ_D and the excitation frequency ω_f equals the circular frequency ω_b of the auxiliary beam. Therefore, Ω_R^{3*} is located near the frequency of resonance of the auxiliary beam. As mentioned in Section 3.4, no amplification of the main beam response is detected in that region of values of Ω when the ranges of interest of the governing parameters are considered.

The solution of interest is Ω_R^{1*}, which leads to the minimum resonant response. From now on, this value will be referred to as the optimal dimensionless excitation frequency

$$\Omega_R^{*} = \frac{1}{2+\mu}\sqrt{(2+\mu)(2+\mu\eta^2)}. \tag{20}$$

Thus, the optimal damping ratio $\zeta_{D,A}^*$ may be computed by enforcing the following condition:

$$\frac{\partial A_B}{\partial \Omega}\left(\Omega = \Omega_R^*, \zeta_D = \zeta_{D,A}^*\right) = 0. \tag{21}$$

The same facts stated above regarding the dynamic amplification A_B also hold for the acceleration a_B. Since Eq. (18) must be satisfied in order for a_B to be independent of ζ_D, Eq. (20) also furnishes the optimal Ω_R^* for the minimum maximum acceleration. The optimal damping ratio which minimises the resonant

acceleration, $\zeta^*_{D,a}$, is given by

$$\frac{\partial a_B}{\partial \Omega}\left(\Omega = \Omega^*_R, \zeta_D = \zeta^*_{D,a}\right) = 0. \tag{22}$$

Each of the Eqs. (21) and (22) presents two identical solutions with opposite signs. The positive ones give the optimal values $\zeta^*_{D,A}$ and $\zeta^*_{D,a}$ for a particular combination of main and auxiliary beams

$$\zeta^*_{D,A} = \frac{(\eta^2 - 1)\mu}{\sqrt{4 + 6\mu + 2\mu^2 + 2\mu\eta^2 + 3\mu^2\eta^2 + \mu^3\eta^2}}, \tag{23a}$$

$$\zeta^*_{D,a} = \frac{(\eta^2 - 1)\mu}{\sqrt{4 + 2\mu + 6\mu\eta^2 + 3\mu^2\eta^2 + 2\mu^2\eta^4 + \mu^3\eta^4}}. \tag{23b}$$

When the damping ratios given by Eqs. (23) are substituted in Eq. (9d), the associated optimal damper constants are obtained when structural damping is regarded as negligible. These equations provide optimum *equivalent* dampers, which are related to a particular longitudinal distribution of FVDs.

The computation of Ω^*_R in the presence of structural damping, in other words, directly from Eq. (13), implies analytically solving for the roots of a bi-quintic polynomial, something proven unfeasible [20]. This fact along with the rather low structural damping values found in modern railway bridges justifies this simplified approach to the optimisation problem. Finally, examples in Section 5 show that Eqs. (23) are appropriate for real cases where structural damping must be considered.

4.2. Vehicle–bridge interaction. Uncertainties in the determination of the mass of the main beam

The determination of the mass per unit length of a railway bridge is affected by two factors that may influence the computed value of the mass and frequency ratios. Therefore, these two factors can alter the optimum value of the supplemental damping ratios predicted by Eqs. (23).

First, the assessment of the real mass of all bridge elements, including ballast, introduces a variability in the modal mass $m_B L/2$ and the natural frequency ω_B of the main beam. This variability, however, should not be of importance if the determination of the masses is carried out with the accuracy required. Besides, if the installation of the FVDs is suitably planned, the natural frequency of the main beam will always be able to be determined experimentally before the damping devices are mounted. Therefore, it will always be possible to obtain the optimal damper constants by applying Eqs. (23).

However, vehicle–bridge interaction is a second factor that must also be taken into account. Vehicle–bridge interaction has been studied by Yang and Yau [21], Yang et al. [22] and Museros and Alarcón [23] among others. These studies have shown that, without taking into account possible effects of wheel or rail irregularities, vehicle–bridge interaction produces three principal effects in resonance situations: (i) a reduction of the bridge response at resonance due to an absorption of energy by the vehicle masses and suspension system; (ii) a reduction of the vertical acceleration of the bridge caused by the presence of the unsprung masses (wheelsets), which augment the effective linear mass m_B; (iii) a reduction of the natural frequency of oscillation of the bridge, and consequently, a reduction of the resonance speed, which is also due to the unsprung masses circulating in contact with the rails. The semi-sprung masses (e.g. bogies or trucks) increment effects (ii) and (iii) whenever their associated natural frequencies are elevated in comparison with the fundamental frequency of the bridge ω_B. In such conditions the semi-sprung masses behave approximately as if they were unsprung. In contrast, the sprung masses or car-bodies have very little influence because their natural frequencies are very low, most of the times with values below 1 Hz.

Since the unsprung and semi-sprung masses increase the effective mass of the bridge, during the passage of a train the mass and frequency ratios will change from the values computed for the unloaded structure. In principle, this could reduce the effectiveness of the optimal dampers predicted by Eqs. (23).

For this reason, it is interesting to determine whether a small increase in the bridge mass per unit length m_B leads to a decrease in the response of the optimally retrofitted bridge when it has been equipped with optimal dampers. If this is the case, then calculating the optimal damper constants by means of Eqs. (23) would always be conservative.

In order to evaluate this condition with an analytical approach, the derivative of the bridge amplification at resonance with respect to m_B should accomplish the following:

$$\frac{\partial}{\partial m_B} A_B\left(\Omega = \Omega_R^*(m_B)\right) \leqslant 0 \quad \text{for} \quad m_B \in \left[m_B^U,\, 1.20\, m_B^U\right], \tag{24}$$

where m_B^U represents the unloaded bridge mass per unit length. The upper limit of the assumed m_B range is due to the fact that, considering the unfavourable hypothesis that two wheelsets and their corresponding bogie are located at mid-span on a short bridge, the increase of the modal mass $m_B L/2$ is expected to be lower than approximately 20%. Substituting Eq. (13a) into Eq. (24)

$$\frac{\partial}{\partial m_B}\left[\sqrt{\frac{4\Omega_R^*(m_B)^2\left(\zeta_b\eta(m_B)\mu(m_B)+\zeta_{D,A}^*\left(m_B^U\right)\right)^2+\mu(m_B)^2\left(\eta(m_B)^2-\Omega_R^*(m_B)^2\right)^2}{E\left(m_B,m_B^U\right)^2+4\Omega_R^*(m_B)^2F\left(m_B,m_B^U\right)^2}}\right]\leqslant 0, \tag{25}$$

where E and F are provided by Eqs. (13c) and (13d), respectively. As the sole computation of $\Omega_R^*(m_B)$ implies solving the roots of a bi-quintic-degree polynomial in terms of Ω, this makes the analytical procedure unfeasible and a numerical approach has been performed instead, which is presented in what follows.

Fig. 6 shows the response of a beam retrofitted with a damping system and subjected to a sinusoidal excitation for which different values of m_B are considered. The lowest value $m_B = 10{,}000\,\text{kg/m}$ represents the mass of the unloaded bridge, whereas increments of m_B up to 20% are used in order to simulate effects (ii) and (iii) mentioned above. The rest of the mechanical characteristics are the following: $L_B = L_b = 15\,\text{m}$, $E_B = 3.6\times10^{10}\,\text{N/m}^2$, $I_B = 0.4531\,\text{m}^4$, $E_b = 2.1\times10^{11}\,\text{N/m}^2$, $I_b = 0.04469\,\text{m}^4$, $m_b = 1546.9\,\text{kg/m}$, $\zeta_B = 0.02$, and $\zeta_b = 0.005$. The solid lines in Fig. 6 represent the response computed using the optimal supplemental damping $\zeta_{D,A}^*$ associated with the initial mass $m_B = 10{,}000\,\text{kg/m}$. This optimal damping is equal to 0.166. As can be seen, although this value of ζ_D is not optimal for other values of m_B, the maximum dynamic amplification diminishes when the linear mass is increased. Evidently, this fact would not be observed if the main beam were not retrofitted, i.e. if it were not connected to the auxiliary one.

Conversely, the discontinuous line in Fig. 6 corresponds to the response of a 12,000 kg/m bridge retrofitted with the optimal damper $\zeta_{D,A}^*$ associated with this mass. The maximum of the discontinuous curve is lower

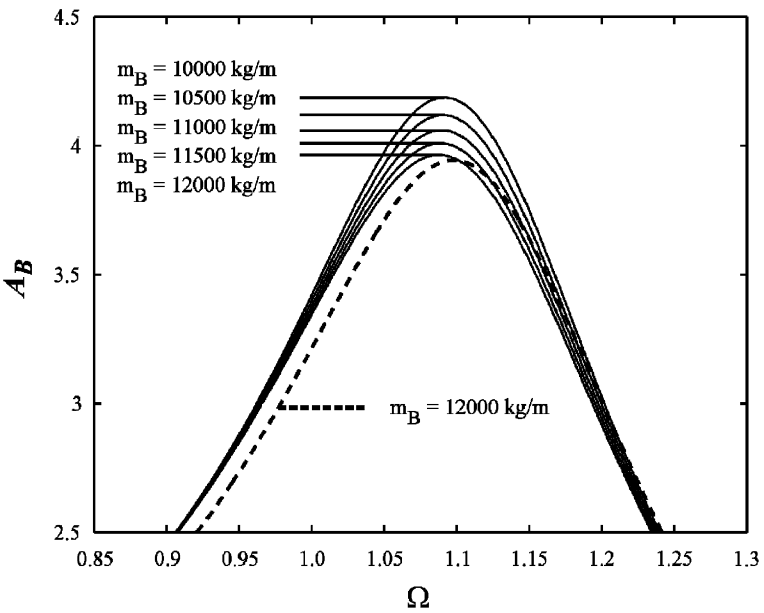

Fig. 6. Main beam amplification versus Ω accounting for mass increments of the main beam up to 20%. ——— Optimal damper associated with $m_B = 10{,}000\,\text{kg/m}$, - - - - optimal damper associated with $m_B = 12000\,\text{kg/m}$.

than the maximum of the solid line corresponding to $m_B = 12{,}000\,\text{kg/m}$. This means that if the optimal damper could be used for each value of linear mass, an even lower amplification would be obtained. However, this cannot be accomplished in practice if the mass increments are due to vehicle–bridge interaction.

Insofar as the maximum vertical acceleration is concerned, this magnitude decreases more rapidly than the amplification if the linear mass is increased. The reason underlying this fact is the existing inverse proportionality between a_B and m_B, (see Eq. (14)). This kind of behaviour is further illustrated in Section 5.4.

In conclusion, it has been shown that an increase of the effective linear mass of the main beam caused by the unsprung and semi-sprung masses of the vehicle will not reduce the effectiveness of the optimal dampers obtained from Eqs. (23). This tendency has been observed in the following ranges of typical values: ($1.25 \leqslant \eta \leqslant 2.5$, $0.05 \leqslant \mu \leqslant 0.25$, $0 \leqslant \zeta_B \leqslant 0.05$, $0 \leqslant \zeta_b \leqslant 0.05$, $0 \leqslant \zeta_D \leqslant 0.20$). The example included in Section 5.4 confirms this conclusion for a real load train circulating over a simply supported bridge at resonance speed.

5. Introduction of the railway traffic excitation

In this section the design methodology proposed is evaluated for its application in simply supported bridges traversed by high-speed trains. The optimal dampers are selected by applying Eqs. (23), and their adequacy for the suppression of the resonant response of the bridge is proven.

5.1. Case studies

Two simply supported bridges are analysed: a 15 m bridge with $m_B = 10{,}000\,\text{kg/m}$, $E_B = 3.6 \times 10^{10}\,\text{N/m}^2$ and $n_{0B} = 8.92\,\text{Hz}$ where n_{0B} is the fundamental natural frequency in Hz, and, a 25 m bridge with $m_B = 16{,}000\,\text{kg/m}$, $E_B = 3.6 \times 10^{10}\,\text{N/m}^2$ and $n_{0B} = 5.80\,\text{Hz}$. In both cases the auxiliary beam is a steel member with a hollow rectangular cross-section, having $L_b = L_B = L$ and $E_b = 2.1 \times 10^{11}\,\text{N/m}^2$. The external dimensions of the auxiliary beam are $b \times h$ (width $\times$ height), and its constant thickness is e. Thus, the second moment of area is $I = (bh^3 - (b-2e)(h-2e)^3)/12$. The mass per unit length is $m_b = \rho_b(bh - (b-2e)(h-2e))$, where $\rho_b = 7850\,\text{kg/m}^3$ is the mass density of steel. Respectively, linear and quadratic variations of b and e in terms of h are adopted

$$b(h) = a \times h \quad \text{for } a = 0.6, \tag{26}$$

$$e(h) = e_0 + e_1 \times h + e_2 \times h^2 \quad \text{for } e_0 = 2.14 \times 10^{-2}\,\text{m},\ e_1 = 7.86 \times 10^{-3},\ e_2 = 1.07 \times 10^{-2}\,\text{m}^{-1}. \tag{27}$$

The dynamic response of each retrofitted bridge due to trains of concentrated loads is calculated by modal superposition, accounting for the first three bending modes of both elements (bridge and auxiliary beam). The assumed modal damping ratios are $\zeta_n^B = 1.35\%$, $n = 1, 2, 3$ in the 15 m case; $\zeta_n^B = 1\%$, $n = 1, 2, 3$ in the 25 m case as stated by Eurocode 1 [24] for pre-stressed concrete bridges; and $\zeta_n^b = 0.5\%$, $n = 1, 2, 3$ for the steel auxiliary beam. Three dampers are introduced that link corresponding sections of the main and auxiliary beams. The dampers are located at mid-span, one quarter and three quarters of span.

The presence of the dampers couples the modal oscillations, as is apparent in Eq. (6). Therefore, in order to verify that all relevant modal contributions are being taken into account, the response of several representative examples has been evaluated considering the first ten modes of the two beams. Both bare and strongly retrofitted configurations as well as resonant and non-resonant conditions have been analysed. From this analysis the authors conclude that including more than three modal contributions does not modify the response of the auxiliary beam in terms of maximum displacements, accelerations, stresses and reactions, or the maximum damper axial forces. In the case of the main beam, only the vertical acceleration experiments a slight variation, but (i) this variation occurs only when the external damping introduced is very high, and high enough to almost or totally eliminate the resonant peak of the main beam fundamental mode; (ii) this variation is associated with high-frequency oscillations corresponding to modes higher than the third one; (iii) the variation relative to the maximum acceleration calculated with three modes is small (less than 9% in all the examples considered); (iv) in a vast majority of cases, accounting for three bending modes of the main beam ensures that the frequency content relevant for the ballast deconsolidation problem of simply supported

bridges is taken into account. For all these reasons, the contribution of three modes for each beam has been considered in what follows.

The modal equations of motion, Eq. (6), are numerically integrated by the Newmark–Beta linear acceleration method. Following the superposition defined by Eq. (2), the vertical displacements, velocities, accelerations and damper forces are computed from the modal amplitudes and their time derivatives. Conversely, the reactions at the supports and bending moments are calculated by the dynamic equilibrium of linear and angular momentum, i.e. applying Euler's Equations (Holzapfel [25]). This procedure captures the influence of the concentrated moving loads, and avoids the Gibbs phenomenon that occurs when the internal forces are computed by modal superposition (Pesterev and Bergman [26]). The expressions used for obtaining the bridge reaction R_{yB} at the first support and the bending moment M_{zB} are

$$R_{yB}(x=0) = \frac{1}{L}\sum_{k=1}^{N_P}\left(H\left(t-\frac{d_k}{V}\right)-H\left(t-\frac{d_k+L}{V}\right)\right)P_k(L-Vt+d_k) + \frac{1}{L}m_B\int_0^L\left[\sum_{j=1}^{N_{\text{mod}}^B}\ddot{\xi}_j^B\,\sin\left(\frac{j\pi x}{L}\right)(L-x)\right]\mathrm{d}x + \frac{1}{L}\sum_{i=1}^{N_D}C_{Di}\dot{y}_{\text{rel},i}(L-x_{Di})+\frac{1}{2}m_BLg, \tag{28a}$$

$$M_{zB}(x_0) = \left(R_{yB}(x=0)-\frac{1}{2}m_BLg\right)x_0-\sum_{k=1}^{N_P}\left(H\left(t-\frac{d_k}{V}\right)-H\left(t-\frac{d_k+x_0}{V}\right)\right) \times P_k(x_0-Vt+d_k)-m_B\int_0^{x_0}\left[\sum_{j=1}^{N_{\text{mod}}^B}\ddot{\xi}_j^B\sin\left(\frac{j\pi x}{L}\right)(x_0-x)\right]\mathrm{d}x - \sum_{i=1}^{N_{D0}}C_{Di}\dot{y}_{\text{rel},i}(x_0-x_{Di}), \tag{28b}$$

where x_0 is a generic section of the bridge, g the acceleration of gravity, and N_{D0} is the number of dampers located between $x=0$ and x_0. The remaining variables retain the meanings defined in Sections 3.1 and 3.2. The bridge reaction at the end support ($x=L$) is computed in an analogous manner. The self-weight is included in the bridge reactions in order to evaluate the tendency of the structure to lose contact with the abutments in resonance condition. In contrast, the self-weight is not included in the bending moment because only the dynamic effects due to the moving loads are to be determined (the same holds for the vertical displacement, computed by modal superposition).

As regards the normal stress and reactions of the auxiliary beam, the self-weight is included in both magnitudes because the feasibility of the retrofitting system is to be proven. The reactions and bending moments of the auxiliary beam are computed by using expressions analogous to Eqs. (28).

Two train load models have been used: the A8 train from the Eurocode 1 High-Speed Load Model [24] in the case of the 15 m bridge, and the Eurostar in the case of the 25 m bridge. The definition of the Eurostar train can be found in Appendix A. The velocities considered range from 40 to 117 m/s in steps of 0.2 m/s (144–421.2 km/h in steps of 0.72 km/h).

5.2. Parametric study between ζ_D and h

Once the main beam characteristics are given, Eqs. (26) and (27) allow expression of the mass and frequency ratio as a function of h. The remaining parameters are fixed except for the external damping and, therefore, it is possible to carry out parametric studies of the response as a function of h and ζ_D.

In this section, different combinations of auxiliary beam sizes and FVD constants are evaluated as possible retrofit alternatives. For the 15 m bridge, the values of h considered range from 0.80 m up to 1.50 m in 1 cm

steps, and the values of ζ_D range from 0% to 35% in 1% steps. Therefore 2556 retrofit alternatives are analysed. For the 25 m bridge, h ranges from 1.25 m up to 2.00 m in 1 cm steps with the same ζ_D pattern. Consequently, 2736 retrofit alternatives are analysed. The range of values selected for h satisfies the condition $\eta > 1$, essential for the effectiveness of the system. For each pair (h, ζ_D), the maximum response is computed in the velocities' range of interest. The supplemental damping ratio is defined according to Eqs. (7) and (9d), assuming equal constants for the three dampers. Therefore, the relation between the FVD constants and ζ_D is

$$\zeta_D = \frac{C_D}{m_B L \omega_B} = \frac{\sum_{i=1}^{N_D} C_{Di} \sin^2(\pi x_{Di}/L)}{m_B L \omega_B} = \frac{C_{D1}}{m_B L \omega_B} \sum_{i=1}^{3} \sin^2\left(\frac{\pi x_{Di}}{L}\right), \quad C_{D1} = C_{D2} = C_{D3}. \tag{29}$$

Except for the reactions, the maximum absolute value of the response variables in the previously mentioned range of velocities is computed. In the case of the reactions, both maximum and minimum values are obtained. The maximum (or minimum) values are represented in contour plots in terms of h and ζ_D. The objectives of this section are (i) to achieve a better understanding of the evolution of the response with the level of external damping introduced; and (ii) to find out whether the analytical optimal damper constants, Eqs. (23), are appropriate for mitigating the resonances generated by real trains, and correlate adequately with the *real*

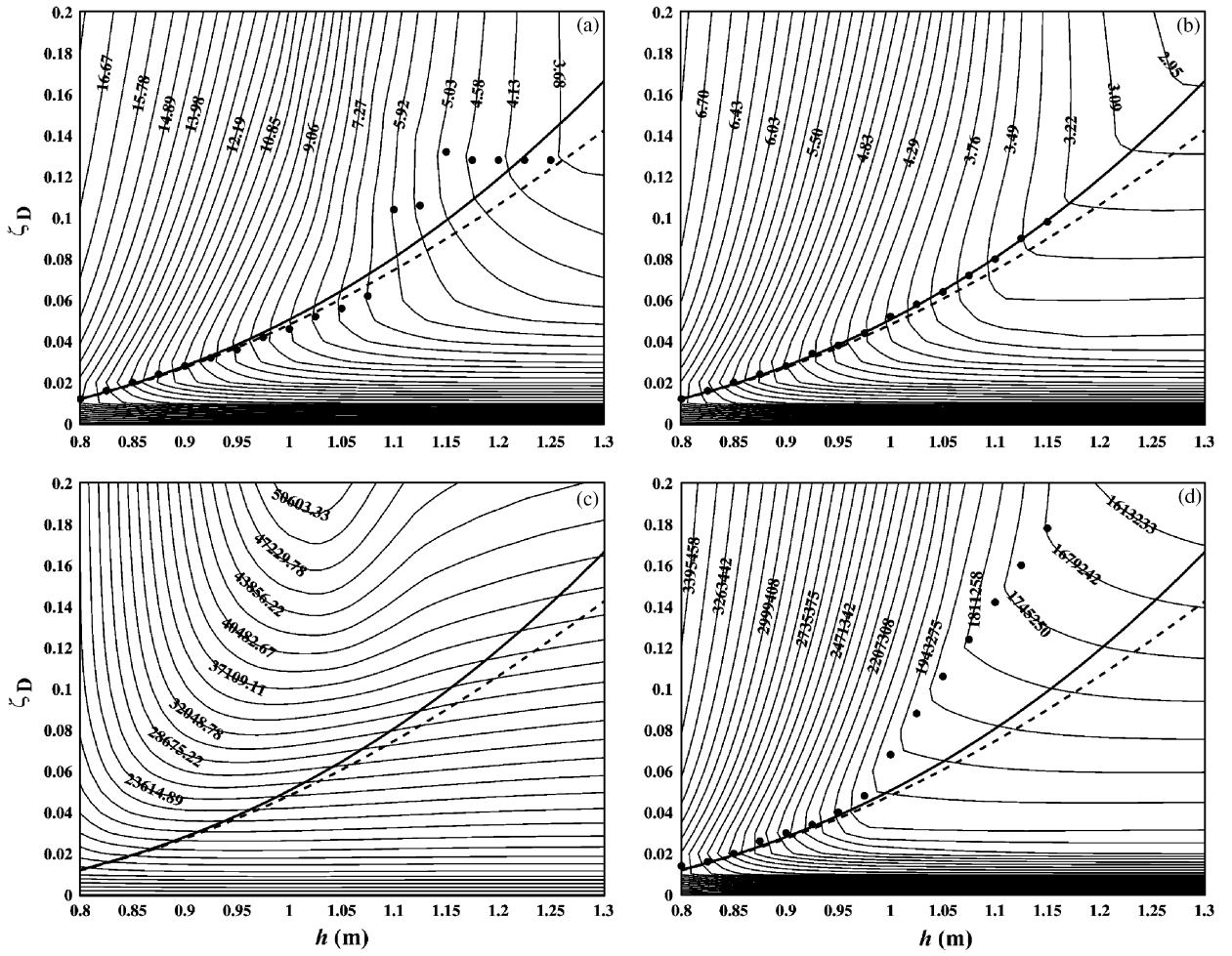

Fig. 7. Response of a 15 m bridge under the circulation of the Eurocode 1 A8 high-speed train: (a) $a_{B,\max}$ (m/s^2) at $x = L/2$, (b) $y_{B,\max}$ (mm) at $x = L/2$, (c) $F_{D,\max}$ (N) at $x = L/2$, (d) $M_{zB,\max}$ (Nm) at $x = L/4$; ● numerical optimal ζ_D, ——— $\zeta^*_{D,A}$, - - - - $\zeta^*_{D,a}$.

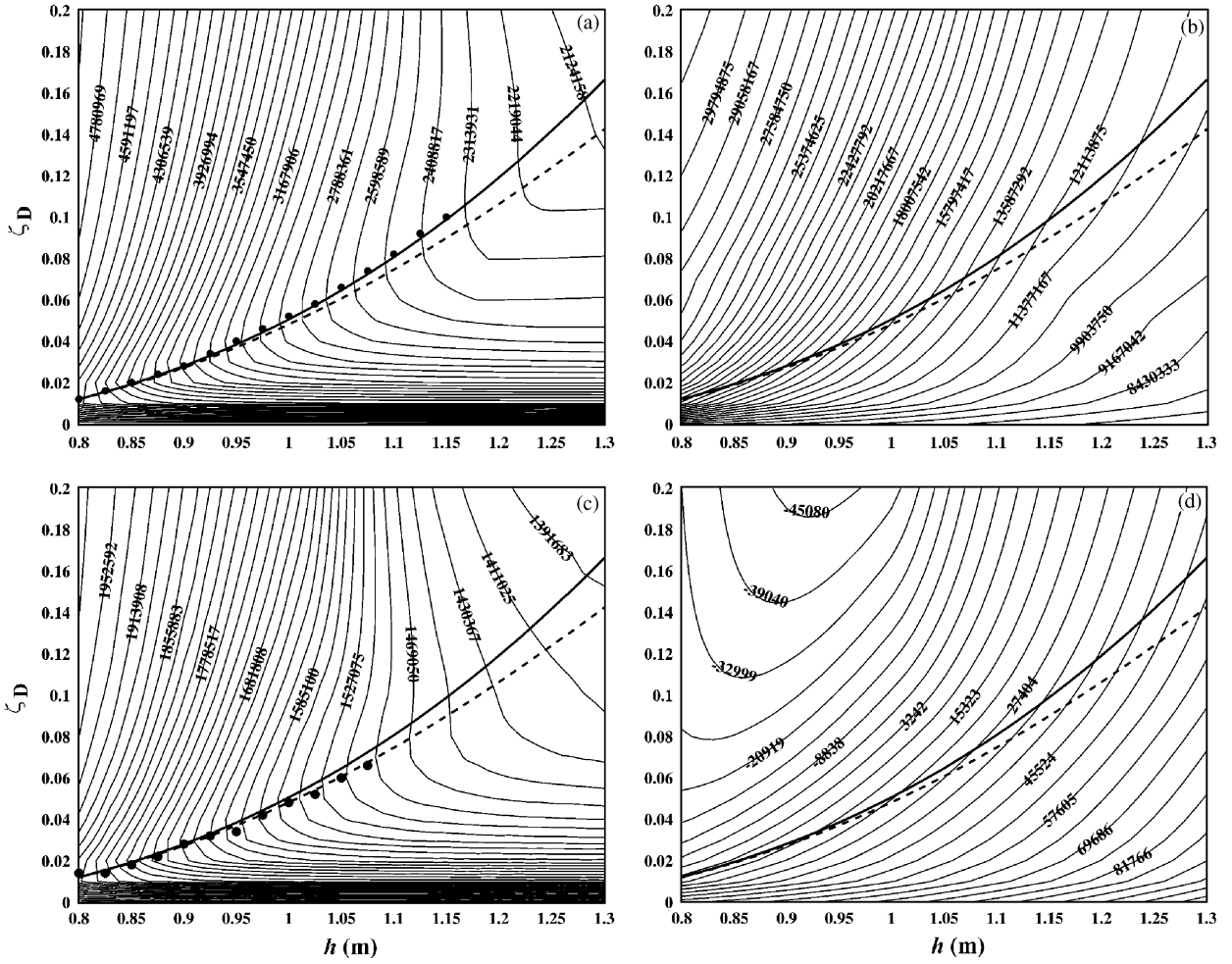

Fig. 8. Response of a 15 m bridge under the circulation of the Eurocode 1 A8 high-speed train (a) $M_{zB,\max}$ (N m) at $x = L/2$, (b) $\sigma_{xb,\max}$ (Pa) at $x = L/2$, (c) $R_{yB,\max}$ (N) at $x = L$, and (d) $R_{yb,\min}$ (N) at $x = L$; ● numerical optimal ζ_D, ——— $\zeta^*_{D,A}$, - - - - $\zeta^*_{D,a}$.

values of the optimal dampers. The real optima are found numerically from the ensemble of the alternatives analysed: for each value of h, a numerical optimum exists for a given h, providing that there is a value of ζ_D leading to a minimum of the response variable.

Figs. 7 and 8 show the response of the 15 m bridge under the A8 high-speed train. Before the retrofitting system is installed, this bridge undergoes a severe second resonance situation (two cycles of oscillation between the passages of consecutive groups of loads) when the A8 train circulates at 403.2 km/h. This resonance induces the maximum acceleration, displacement and bending moment. In each graph, the analytical optimal supplemental damping ratios $\zeta^*_{D,A}$ and $\zeta^*_{D,a}$, obtained from Eqs. (23), have been plotted in terms of h. Providing that they exist, the numerical or real optimum pairs (h, ζ_D) are represented with black dots for discrete values of h.

Figs. 7a and 7b show the maximum vertical acceleration $a_{B,\max}$ and displacement $y_{B,\max}$ at the bridge mid-span. As can be seen, a numerical optimum can be found for all but the highest values of h. From Figs. 7a and 7b it may be inferred that for very stiff auxiliary beams, increasing the damper constants leads to a remarkable reduction of the response because the beam tends to be a rigid reference for the damper. In contrast, for small values of h increasing the damper constants is not efficient because the auxiliary beam is too flexible. It is worth mentioning as well that the analytical and numerical optimal damping ratio paths do not direct towards the maximum damper force ($F_{D,\max}$) levels (see Fig. 7c), but to the maximum reduction of the bridge response.

The FVDs introduce punctual loads, i.e. localised shear that the bridge must be prepared to withstand. This means that a detailed study of the connections will be required for each particular case. Nevertheless, it should be stressed at this point that the maximum damper forces required for a satisfactory reduction of the acceleration and displacement are of the order of 40 or 50 kN (see Fig. 7c), which is perfectly bearable by common reinforced concrete slabs such as the ones used in most girder bridges. Typical maximum punching loads for this kind of slab reaches values of 100–200 kN.

In order to account for the maximum stresses in the bridge (i.e. the maximum bending moment at mid-span), a quarter and three quarters of span has been evaluated. The maximum bending moment $M_{zB,\max}$ at a quarter of span and at mid-span is shown in Figs. 7d and 8a, respectively. Both figures are similar to the bridge acceleration and displacement plots. More specifically, there is an evident similarity between Figs. 7b and 8a while Fig. 7d is slightly different, which is a consequence of the influence of the second and third bending modes.

The maximum normal stress at the mid-span section of the auxiliary beam $\sigma_{xb,\max}$, including its self weight, is shown in Fig. 8b. Though not included as a figure, the beam bending moment increases along any of the two optimal damping curves towards improved bridge performances, which is due to the increasing forces exerted by the dampers. However, the effect of the height of the beam in the reduction of the normal stress is stronger than the increase in the bending moment and, therefore, the normal stress reduces along the analytical optimal damping curves.

Fig. 8c shows that the maximum bridge vertical reactions $R_{yB,\max}$ follow a pattern very similar to the rest of the bridge responses. This is a fact that holds for both end supports. As for the auxiliary beam vertical reactions, very low values of these magnitudes are undesirable as they may lead to a loss of contact with the abutments. Should that occur, a connection designed for bearing the traction forces would have to be used. As shown in Fig. 8d, the worst situation occurs when high damping is combined with a very flexible auxiliary beam. In any case, since these points in the contour graph are not optimal for bridge performance, they are not to be expected. The behaviour of the minimum vertical reaction with h and ζ_D is somewhat similar to that of the normal stress because as the beam size and ζ_D increase, higher upward forces act on the beam. However, the increase in self weight compensates for this effect.

Figs. 9 and 10 show the response of the 25 m bridge under the circulation of the Eurostar high-speed train. This train induces a first resonance at 403.2 km/h, which equals the speed of the second resonance in the case of the 15 m bridge. In a first resonance situation only one cycle of oscillation of the bridge takes place between the passages of consecutive groups of loads. The evolution of the different response variables is very similar to the results obtained for the 15 m bridge under the A8 train. The most significant differences are the following: (i) the bending moment $M_{zB,\max}$ at one quarter of span is more similar to the bending moment at mid-span, which evidences a weaker influence of the second and third bending modes; (ii) the minimum reaction of the auxiliary beam $R_{yb,\min}$ always remains positive.

Finally, Figs. 7–10 show that the numerical optimal values of ζ_D for the bridge displacement and bending moments correlate better with $\zeta^*_{D,A}$ while the acceleration and bridge reactions do so with $\zeta^*_{D,a}$. The difference between both analytical optimal damping curves is remarkably small, especially for low values of h. The agreement between the numerical and analytical optima is very good until $h = 1.1$ m in the case of the 15 m bridge or until $h = 1.7$ m in the case of the 25 m bridge. The reason why the numerical optima start to diverge from the analytical ones is that for high values of h and ζ_D, a large amount of damping is introduced in the system, and the resonant peak is suppressed (see Figs. 11a and b). In such conditions the maximum of the response does not occur in resonance anymore, but normally takes place at the maximum speed $V = 420$ km/h. Therefore, the analytical optimal ζ_D obtained from the sinusoidal excitation is no longer accurate. In any case, the amount of damping needed for the vanishing of the resonant peaks is quite large, and leads to substantial reductions of the bridge response.

5.3. Performance of the retrofitted bridges

In this section, the bare and retrofitted behaviours of the two bridges under study are compared. Studies from the European Rail Research Institute have brought to light that the control of vertical accelerations is of paramount importance for short high-speed bridges. Consequently, in all cases h is associated with its

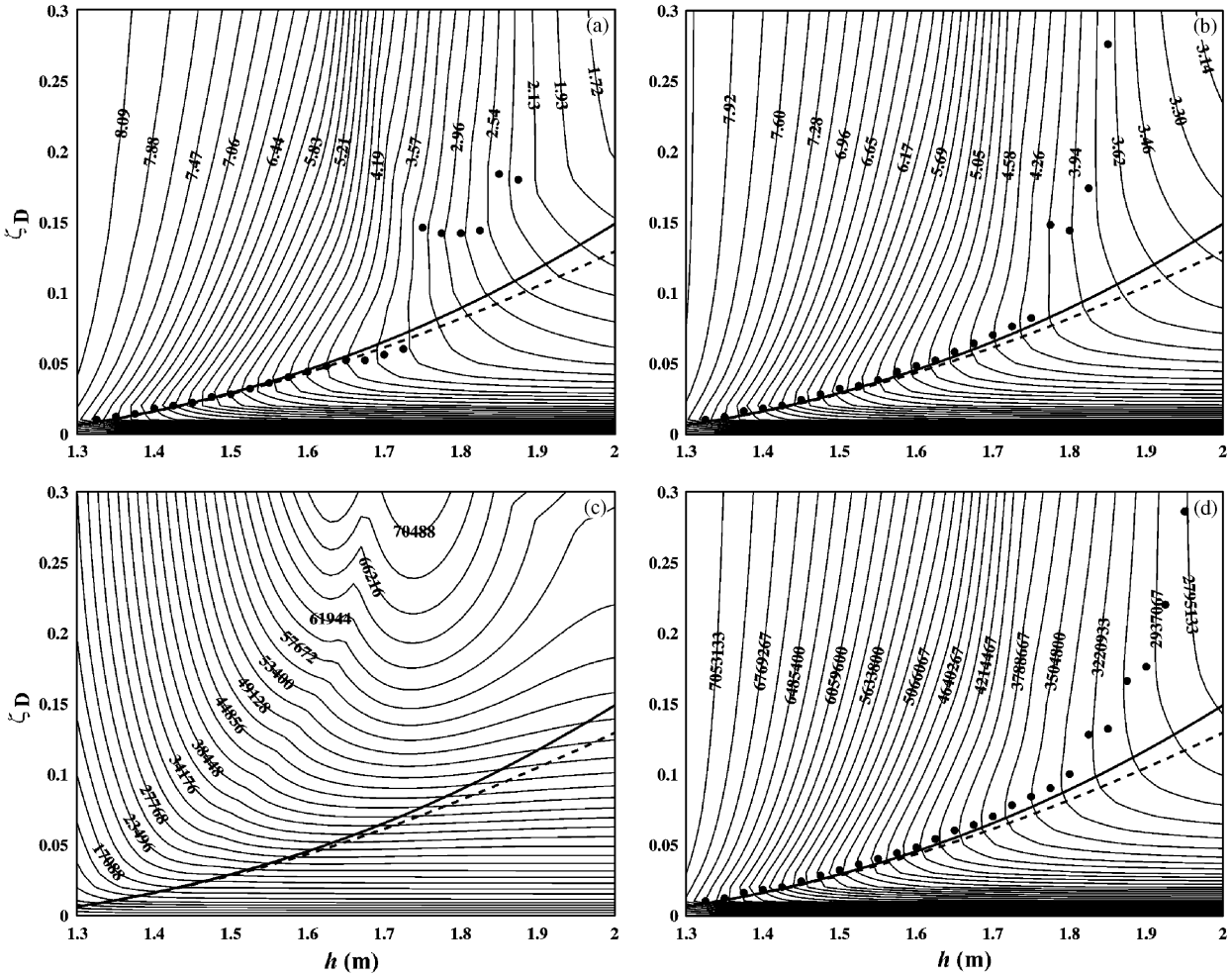

Fig. 9. Response of a 25m bridge under the circulation of the Eurostar high-speed train: (a) $a_{B,\max}$ (m/s^2) at $x = L/2$, (b) $y_{B,\max}$ (mm) at $x = L/2$, (c) $F_{D,\max}$ (N) at $x = L/2$, (d) $M_{zB,\max}$ (N m) at $x = L/4$; ● numerical optimal ζ_D, ——— $\zeta^*_{D,A}$, - - - - $\zeta^*_{D,a}$.

analytical optimal damping derived from the acceleration $\zeta^*_{D,a}$. Two levels of retrofit are selected: (i) a level such that the Eurocode [27] target acceleration requirement is achieved (3.5 m/s^2 for ballasted bridges); (ii) an intermediate level leading to a less severe retrofit option. The constants of the three dampers are computed by means of Eq. (23b), taking into account Eqs. (26), (27) and (29).

Figs. 11a–11f show the 15 m bridge response under the A8 load train as a function of the speed. This train induces a second and third resonance of the first flexural mode of the bridge at 112 m/s (403.2 km/h) and at 74 m/s (266.4 km/h), respectively. The maximum vertical acceleration of the bare structure is 18.4 m/s^2. In order to reduce this acceleration to less than 3.5 m/s^2 a beam height of 1.3 m has been selected, which when combined with the optimal damper given by expression (23b) leads to 3.52 m/s^2 at mid-span. In this case the theoretical values of the dissipative system are $\zeta^*_{D,a} = 14.2\%$ and $C_{Di} = 597\,801$ N s/m for $i = 1, 2, 3$. The maximum response of the bridge has also been computed for a less severe dissipative system with $h = 1$ m. In this case $\zeta^*_{D,a} = 4.8\%$, $C_{Di} = 202\,153$ Ns/m for $i = 1, 2, 3$, and the maximum acceleration at mid-span reduces to 7.71 m/s^2. The maximum vertical displacement at mid-span is shown in Fig. 11b. It reduces from 7.37 mm in the unretrofitted case to 3.99 mm for $h = 1$ m, and to 3.04 mm for $h = 1.3$ m.

These results are obtained along with the damper axial forces shown in Fig. 11c. The damper located at mid-span maximum force reaches 23.7 kN for $h = 1$ m and 38.0 kN in the $h = 1.3$ m case, which is far below the

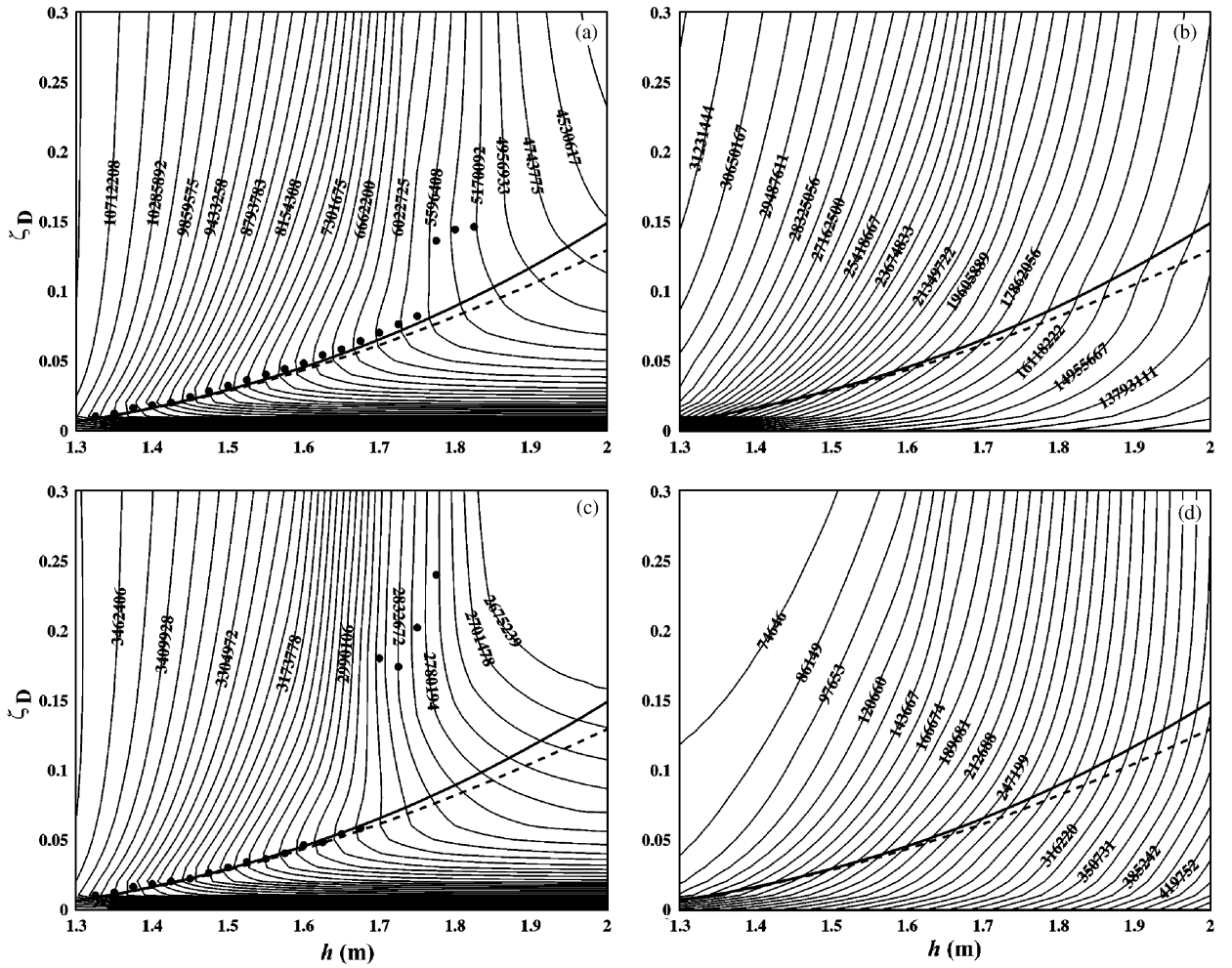

Fig. 10. Response of a 25 m bridge under the circulation of the Eurostar high-speed train: (a) $M_{zB,\max}$ (Nm) at $x = L/2$, (b) $\sigma_{xb,\max}$ (Pa) at $x = L/2$, (c) $R_{yB,\max}$ (N) at $x = L$, (d) $R_{yb,\min}$ (N) at $x = L$; ● numerical optimal ζ_D, ——— $\zeta^*_{D,A}$, - - - - $\zeta^*_{D,a}$.

present commercial FVD force capacity. The corresponding plot for the damper located at a quarter of span also appears in the same graph. In Fig. 11d the maximum and minimum bridge reactions ($R_{yB,\max}$ and $R_{yB,\min}$) at $x = L$ are shown. The maximum reaction decreases substantially when external damping is added to the system, and the minimum value, which falls below zero in the unretrofitted structure, remains close to the static reaction after retrofitting. The static value indicated in Figs. 11d and e is exclusively due to the self-weight. As regards the reactions of the auxiliary beam (Fig. 11e), it is of interest (though not essential) that the minimum reactions of the auxiliary beam remain positive because, otherwise, tractions would appear in the connection with the abutment. As Fig. 11e shows, even in the $h = 1.3$ m case, when a larger dispersion from the static value appears, the weight of the beam is much larger and, therefore, the reactions do not approach zero. Finally, can be observed in Fig. 11f, the maximum normal stress in the beam is 14.9 in the $h = 1$ m case and 10.5 MPa in the $h = 1.3$ m case, which is far below typical steel yielding stress values.

Figs. 12a–f summarise the comparative response of the 25 m bridge under the Eurostar train. When resonance takes place at 112 m/s (403.2 km/h), the original maximum bridge vertical acceleration reaches 8.91 m/s^2. In order to achieve the target acceleration performance a retrofit alternative with $h = 1.7$ m has been selected. When this auxiliary beam is associated with the theoretical optimal dampers, $\zeta^*_{D,a} = 6.1\%$ and $C_{Di} = 445\,802$ N s/m for $i = 1, 2, 3$, a maximum mid-span acceleration of 3.52 m/s^2 is achieved. The results for

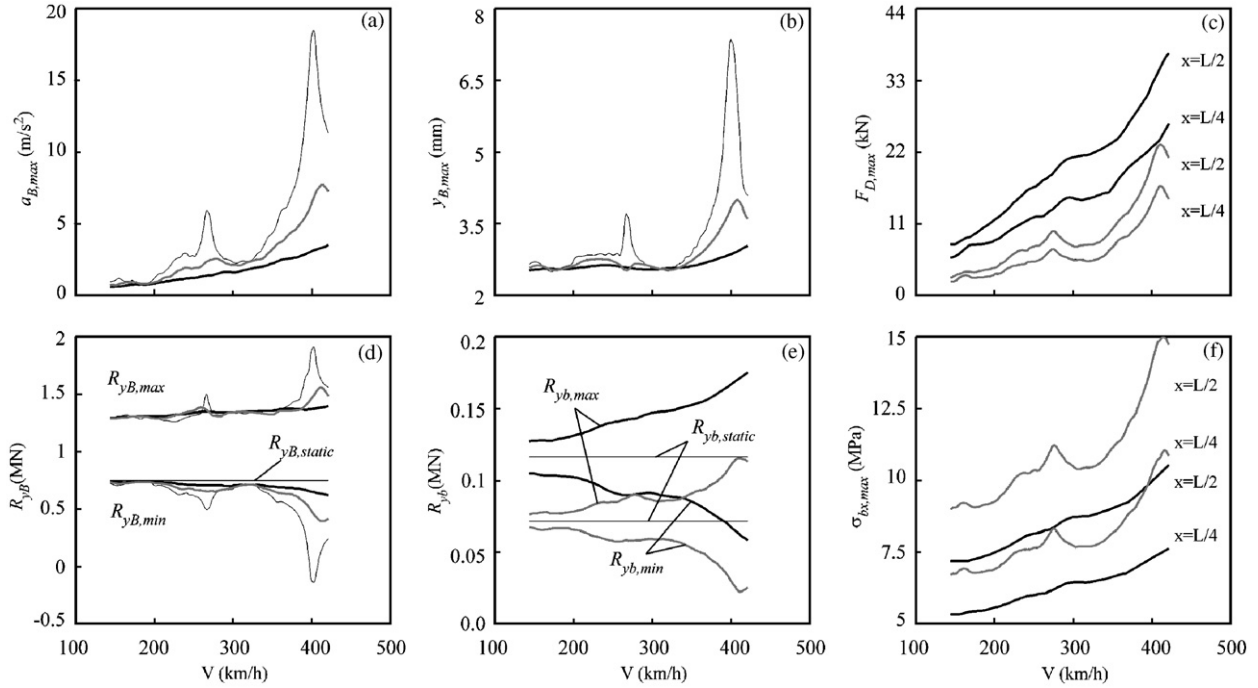

Fig. 11. Response of a 15m bridge under the A8 train: (a) $a_{B,\max}$ at $x = L/2$, (b) $y_{B,\max}$ at $x = L/2$, (c) $F_{D,\max}$, (d) R_{yB} at $x = L$, (e) R_{yb} at $x = L$, (f) $\sigma_{xb,\max}$ at $x = L/2$. —— unretrofitted, ▬ retrofitted ($h = 1$ m), ▬ retrofitted for approximate target performance $a_{\max} = 3.5\,\mathrm{m/s^2}$ ($h = 1.3$ m).

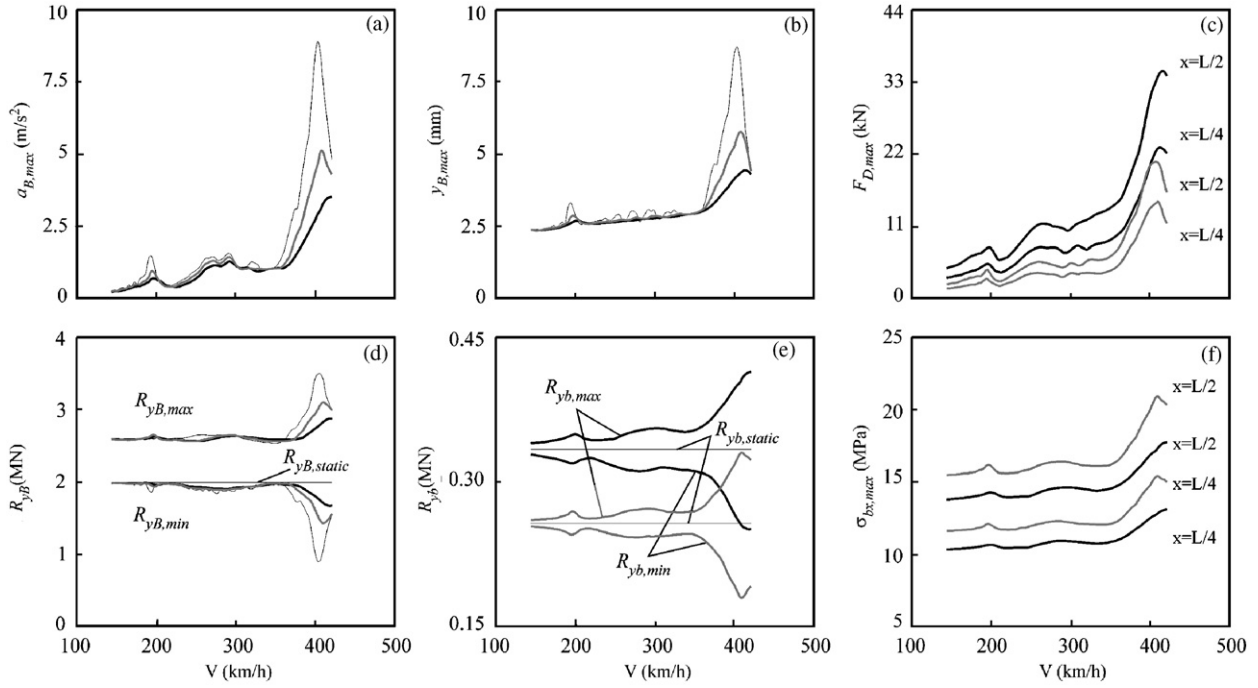

Fig. 12. Response of a 25m bridge under the Eurostar train: (a) $a_{B,\max}$ at $x = L/2$, (b) $y_{B,\max}$ at $x = L/2$, (c) $F_{D,\max}$, (d) R_{yB} at $x = L$, (e) R_{yb} at $x = L$, (f) $\sigma_{xb,\max}$ at $x = L/2$. —— unretrofitted, ▬ retrofitted ($h = 1.5$ m), ▬ retrofitted for approximate target performance $a_{B,\max} = 3.5\,\mathrm{m/s^2}$ ($h = 1.7$ m).

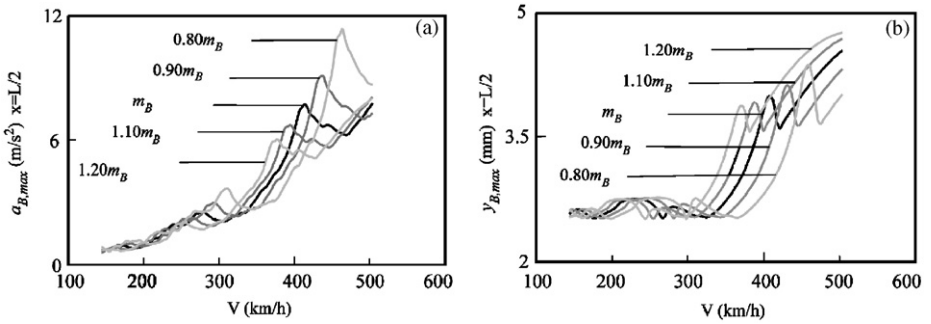

Fig. 13. Response of a 15 m retrofitted bridge ($h = 1$ m) under the A8 train accounting for possible variations of m_B due to interaction effects: (a) maximum bridge mid-span acceleration, (b) maximum bridge mid-span displacement.

an intermediate case with $h = 1.5$ m are also included in the figure. The maximum force experimented by the dampers in the $h = 1.7$ m case is 35.4 kN, which is perfectly acceptable, just like the maximum normal stress in the mid-span section of the auxiliary beam, 17.7 MPa, for the same retrofit option.

5.4. Influence of vehicle–bridge interaction in real cases

Recalling Section 4.2, the effective mass of the main beam may be slightly higher than its theoretical value due to vehicle–bridge interaction effects, which are not accounted for in the optimal equivalent damper derivation. In this section, a numerical test is performed similar to that described in Section 4.2, but for a real bridge and load train excitation.

Fig. 13 shows the response in terms of maximum vertical acceleration and displacement of the previously mentioned 15 m bridge, retrofitted with an auxiliary beam of $h = 1$ m, where h is associated with its analytical optimal damping derived from $\zeta^*_{D,a}$ for the theoretical $m_B = 10{,}000$ kg/m. While keeping the same auxiliary beam and dampers in all the cases, the bridge response under the circulation of the A8 train has been calculated for variations of the main beam mass from $0.8m_B$ to $1.2m_B$. The main conclusion that can be derived from the figure is the same as in Section 4.2. In other words, the maximum bridge response reduces with the increase in its mass even though the damper is optimised for the bridge theoretical mass (that is, disregarding vehicle–bridge interaction). The reduction of the acceleration is stronger than the reduction of the displacement, which is a direct consequence of Newton's second law.

6. Conclusions

The dynamic behaviour of simply supported beams equipped with FVDs and subjected to moving loads has been evaluated in this research study. The proposed damping system consists of a simply supported auxiliary beam placed parallel to the main beam (which supports the passage of the moving loads) and a set of FVDs linking both beams at several sections. From the results obtained in our research, the following conclusions can be derived:

(i) The resonant vibrations that may appear in simply supported beams when subjected to moving loads can be drastically reduced with the damping system proposed here. In the case of railway bridges, the numerical examples presented show that the response can be rendered satisfactory without exceeding the dampers' force capacity, or without exceeding the maximum yielding stress of the auxiliary beam or the punching load capacity of the main beam.
(ii) For a particular auxiliary beam, there exists an optimum value of the FVD constants that minimise the main beam response.
(iii) The design strategy should be to select the smallest auxiliary beam such that when the beam is associated with its corresponding optimal FVDs, this will lead to the desired system performance.

(iv) Analytical expressions for the optimal damper constants are provided which lead to very accurate results as long as the maximum response of the main beam in the range of evaluated velocities occurs at resonance.
(v) With the system proposed in this article the FVDs need not interact with the upper side of the bridge. This allows existing railway bridges to be retrofitted while keeping the line in operation.
(vi) The damping system and optimal damper expressions presented here may apply to other situations where simply supported beams vibrate at resonance due to different causes.

Finally, it should be underlined that only the contribution of flexural modes has been accounted for. Consequently, the results of our study are applicable to structures that essentially behave as simply supported beams. For structures that exhibit torsional oscillations or more complicated three-dimensional behaviour, it will be necessary to use mechanical models different from the one considered here.

Acknowledgements

The authors wish to acknowledge the financial support of the Spanish Ministry of Public Works, in the framework of the National programme for Construction (Area of Transportation and Construction) of the National Plan for Scientific Research, Development and Technological Innovation 2004–2007, under research project No. 80021/A04. The authors are also grateful to Taylor Devices Inc. for the technical information provided, which has proven in valuable in the assessment of the feasibility of the proposed retrofitting system.

Appendix A. Definition of the Eurostar train

The Eurostar train consists of 48 identical 170 kN loads. Table A1 shows the distances between each load and the first load of the train.

Table A1
Definition of load train Eurostar

Load number	Distance (m)	Load number	Distance (m)
1	0.000	25	195.095
2	3.000	26	198.095
3	14.000	27	213.795
4	17.000	28	216.795
5	20.275	29	232.495
6	23.275	30	235.495
7	38.975	31	251.195
8	41.975	32	254.195
9	57.675	33	269.895
10	60.675	34	272.895
11	76.375	35	288.595
12	79.375	36	291.595
13	95.075	37	307.295
14	98.075	38	310.295
15	113.775	39	325.995
16	116.775	40	328.995
17	132.475	41	344.695
18	135.475	42	347.695
19	151.175	43	363.395
20	154.175	44	366.395
21	169.875	45	369.67
22	172.875	46	372.670
23	188.575	47	383.670
24	191.575	48	386.670

References

[1] L. Frýba, A rough assessment of railway bridges for high speed trains, *Engineering Structures* 23 (2001) 548–556.
[2] L. Frýba, Dynamic behaviour of bridges due to high-speed trains, *Workshop Bridges for High-Speed Railways*, Porto, June 2004, pp. 137–158.
[3] F. Mancel, Cedypia: analytical software for calculating dynamic effects on railway bridges, *Proceedings of the Fourth European Conference on Structural Dynamics* (*Eurodyn '99*), Vol. 2, Prague, June 1999, pp. 675–680.
[4] H.C. Kwon, M.C. Kim, I.W. Lee, Vibration control of bridges under moving loads, *Computers & Structures* 66 (1998) 473–480.
[5] J.F. Wang, C.C. Lin, B.L. Chen, Vibration suppression for high-speed railway bridges using tuned mass dampers, *International Journal of Solids and Structures* 40 (2003) 465–491.
[6] J.D. Yau, Y.B. Yang, Vibration reduction for cable-stayed bridges travelled by high-speed trains, *Finite Elements in Analysis and Design* 40 (2004) 341–359.
[7] A.K. Das, S.S. Dey, Effects of tuned mass dampers on random response of bridges, *Computers & Structures* 43 (1992) 745–750.
[8] J.P. Hartog, *Mechanical Vibrations*, fourth ed., McGraw-Hill, New York, 1956.
[9] L.S. Minsili, T. Zhong, H. Xia, D.E. Manguelle, Design and vibration control by friction dampers in truss bridges, *Proceeding of the Second International Conference on Construction in Developing Countries: Challenges Facing the Construction Industry in Developing Countries*, Botswana, November 2002.
[10] J.F. Choo, H.M. Koh, S.C. Kang, B.S. Kim, Vibration control of long-span high-speed railway bridges under periodic moving loading using viscoelastic damper, *Structures for High-speed Railway Transportation*, International Association for Bridge and Structural Engineering, Antwerp (Belgium), June 2003.
[11] G. Oliveto, A. Santini, E. Tripodi, Complex modal analysis of a flexural vibrating beam with viscous end conditions, *Journal of Sound and Vibration* 200 (1997) 327–345.
[12] A. Greco, A. Santini, Dynamic response of a flexural non-classically damped continuous beam under moving loadings, *Computers & Structures* 80 (2002) 1945–1953.
[13] S. Krenk, Complex modes and frequencies in damped structural vibrations, *Journal of Sound and Vibration* 270 (2004) 981–996.
[14] J.A. Main, S. Krenk, Efficiency and tuning of viscous dampers on discrete systems, *Journal of Sound and Vibration* 286 (2005) 97–122.
[15] L. Frýba, *Dynamics of Solids and Structures Under Moving Loads*, third ed., Thomas Telford, London, 1999.
[16] M. Olsson, On the fundamental moving load problem, *Journal of Sound and Vibration* 145 (1991) 299–307.
[17] Y.B. Yang, J.D. Yau, L.C. Hsu, Vibration of simple beams due to trains moving at high speeds, *Engineering Structures* 19 (1997) 936–944.
[18] P. Museros, E. Alarcón, Influence of the second bending mode on the response of high-speed bridges at resonance, *Journal of Structural Engineering* 131 (2005) 405–415.
[19] European Rail Research Institute D-214 Committee, Ponts-Rails pour vitesses >200 km/h, Rapport Final, 2001 (in French).
[20] R.S. Irving, *Integers, Polynomials and Rings*, Springer, New York, 2004.
[21] Y.B. Yang, J.D. Yau, Vehicle–bridge interaction element for dynamic analysis, *Journal of Structural Engineering* 123 (1997) 1512−1518.
[22] Y.B. Yang, J.D. Yau, Y.S. Wu, *Vehicle–bridge Interaction Dynamics with Applications to High-Speed Railways*, World Scientific, Singapore, 2004.
[23] P. Museros, E. Alarcón, An investigation on the importance of train−bridge interaction at resonance, *Proceedings of the Sixth International Conference on Computational Structures Technology*, Prague, September 2002, pp. 335–336.
[24] European Committee for Standardisation (CEN), Eurocode 1: Actions on structures. Part 2: General actions—Traffic loads on bridges. Final Draft prEN 1991–1992 (pre-European Standard), 2002.
[25] G.A. Holzapfel, *Nonlinear Solid Mechanics: A Continuum Approach for Engineering*, Wiley, New York, 2000.
[26] A.V. Pesterev, L.A. Bergman, An improved series expansion of the solution to the moving oscillator problem, *Journal of Vibration and Acoustics* 122 (2000) 54–61.
[27] European Committee for Standardisation (CEN), Eurocode: Basis of Structural Design. Annex A2: Application for bridges, Final PT Draft EN 1990—prAnnex A2 (pre-European Standard), 2002.